Available online at www.sciencedirect.com
SCIENCE DIRECT
Finite Elements in Analysis and Design 42 (2006) 580–591
FINITE ELEMENTS IN ANALYSIS AND DESIGN
www.elsevier.com/locate/finel

A variational multiscale stabilized finite element method for the Stokes flow problem

Xiaohu Liu*, Shaofan Li

Department of Civil and Environmental Engineering, University of California, Berkeley, CA 94720, USA

Received 22 August 2005; received in revised form 22 August 2005; accepted 20 November 2005
Available online 10 January 2006

Abstract

A new stabilized method is proposed for the 2-D Stokes flow problem. The new approach is based on the Variational Multiscale(VM) formulation. The Green's functions for an infinite domain are adopted to compute the two-scale interaction. The method is shown to be able to stabilized low order Finite Element intepolation pairs and has a formulation similar to the one of Galerkin/Least-squares(GLS) formulation. The stabilization term obtained in this method has a physical interpretation. A couple of numerical examples show the method has a good convergence rate.

Keywords: Variational multiscale method; Stabilized method; Stokes method; Green's functions

1. Introduction

Finite element methods (FEMs) have been widely used in solving incompressible fluid flow problems, especially the Stokes problem. However, for the usual velocity–pressure Galerkin formulation to work, it must satisfy a stability condition called the LBB condition. And it is well known that the LBB condition does not hold for low-order velocity–pressure elements. To overcome this problem, the so-called class of stabilized methods has been developed over recent years. Among them are the streamline upwind/Petrov–Galerkin (SUPG) method [1] and the Galerkin/least-squares method [2]. The latter one perturbs the original Galerkin formulation by adding mesh-dependent terms so as to improve stability. However, the stabilized methods often involve some stabilization parameters, whose exact values in general cannot be derived through a systematic way.

The variational multiscale method, proposed by Hughes [3,4], offers a new perspective for the stabilized methods. The starting point of the variational multiscale method is to decompose the solution into two scales: $u = \bar{u} + u'$. Then the method tries to determine u' analytically and $\bar{u}$ numerically. Hughes showed [3] that the stabilization parameter can be derived from the variational multiscale formulation. Hauke applied the method to the 1-D advection-reaction and advection–diffusion-reaction problem to obtained an explicit expression for the stabilization parameter [5].

The variational multiscale method has since become a hot research topic and has been applied to various areas such as large eddy simulations [6], strain localization problems [7] and multiphase flow in porous media [8].

The success of the variational multiscale method resides in solving the fine scale solution analytically. The key factor in determining the fine scale solution is the Green's function used. From the finite element method point of view, we want the fine scale solution to be *locally defined*, thus we need the Green's function to vanish on the boundaries of some local domains. Most of the previous work [3–5] adopt element Green's functions, i.e. Green's functions that vanish on the boundaries of the finite elements. This kind of Green's functions can be found for some 1-D problems [5]. But given the irregularity of a general 2-D or 3-D finite element, it is impossible to find element Green's functions in general. To circumvent this problem, some numerical Green's functions, for example bubble functions,

* Corresponding author. Tel.: +1 5106979185.
E-mail address: xhliu@berkeley.edu (X. Liu).

0168-874X/$ - see front matter © 2005 Elsevier B.V. All rights reserved.
doi:10.1016/j.finel.2005.11.006

are adopted. The drawback of the numerical Green's functions is that they usually do not satisfy the governing PDEs and thus will not lead to a good fine scale solution. In the recent work by the present authors [9,10], we proposed to adopt the Green's functions of an infinite domain. One obvious advantage of this approach is that infinite Green's functions can be found for many real problems. The tradeoff is that infinite Green's functions do not vanish on element boundaries. Regarding this issue, we made the approximation by *neglecting* the fine scale solutions on the boundary. We applied this approach to the linear elasticity problem and via the techniques used in micromechanics inclusion theory, we were able to obtain an explicit fine scale solution. The numerical examples studied yield satisfactory results, thus justified the infinite Green's functions approach to some degree.

In this paper, we apply the variational multiscale framework to the 2-D Stokes flow problem to develop the variational multiscale stabilized (VMS) method. By adopting the infinite Green's function, we determine the fine scale velocity and pressure analytically. We will concentrate on the low-order finite elements, i.e. elements with interpolation order less than 2. It will be shown that the VMS method can lead to a modified weak form similar to the one obtained by the GLS method. But the stabilized term now has a solid physical interpretation, which is the interaction between fine scale velocity and coarse scale pressure. Furthermore, an explicit stabilization parameter matrix is obtained. The numerical results show that the originally unstable elements now become stable.

This paper is organized as follows. In Section 2 we give a brief review of the Stokes problem and the GLS method. In Section 3 we shall present the VMS method. We will start from the multiscale decomposition and then derive the fine scale solution. We will also give the formulations for finite element implementation. Two representative numerical examples are carried out in Section 4 to show the competence of the VMS elements. We will conclude our presentation in Section 5 with a few comments and also possible future research topics.

2. The Stokes problem and its treatment

The Stokes problem is the approximation of the incompressible Navier–Stokes equations in the case of low Reynolds numbers [11]. For the sake of simplicity, in the paper we will consider the Stokes problem with a pure Dirichlet boundary. The strong form of the problem reads

$$-\nu\nabla^2\mathbf{v} + \nabla p = \mathbf{b} \quad \text{in } \Omega, \tag{1}$$

$$\nabla\cdot\mathbf{v} = 0 \quad \text{in } \Omega, \tag{2}$$

$$\mathbf{v} = \mathbf{v}^0 \quad \text{on } \Gamma, \tag{3}$$

where $\mathbf{v}$ is the velocity, p is the kinematic pressure, $\mathbf{b}$ is the body force per unit mass and ν is the kinematic viscosity. Here, $\mathbf{v}$ and p are independent unknowns.

The weak form of the problem can be written as follows:
Find $\mathbf{v}\in\mathscr{S}$ *and* $p\in\mathscr{Q}$ *such that*

$$\begin{aligned}&\int_\Omega \nabla^s\mathbf{w} : \nu\nabla^s\mathbf{v}\,\mathrm{d}\Omega - \int_\Omega p\nabla\cdot\mathbf{w}\\ &\quad = \int_\Omega \mathbf{w}\cdot\mathbf{b}\,\mathrm{d}\Omega \qquad \forall\mathbf{w}\in\mathscr{V}\ \ \forall q\in\mathscr{Q},\\ &\int_\Omega q\nabla\cdot\mathbf{v}\,\mathrm{d}\Omega = 0\end{aligned} \tag{4}$$

where

$$\nabla^s = \tfrac{1}{2}(\nabla + \nabla^{\mathrm{T}}).$$

The corresponding function spaces are defined as

$$\mathscr{S} = \{\mathbf{v}\in[H^1(\Omega)]^2 | \mathbf{v} = \mathbf{v}^0 \text{ on } \Gamma\}, \tag{5}$$

$$\mathscr{V} = \{\mathbf{w}\in[H^1(\Omega)]^2 | \mathbf{w} = 0 \text{ on } \Gamma\}, \tag{6}$$

$$\mathscr{Q} = L^2(\Omega)/\mathbb{R}. \tag{7}$$

Here standard notations from functional analysis are adopted. Readers can consult [12] for details.

Remark 2.1. Please note that the pressure space is taken as $L^2(\Omega)/\mathbb{R}$ because it is known that in the case of pure Dirichlet boundary, the pressure can only be determined up to a constant [13].

If we define two bilinear forms:

$$a(\mathbf{w},\mathbf{v}) = \int_\Omega \nabla^s\mathbf{w} : \nu\nabla^s\mathbf{v}\,\mathrm{d}\Omega, \tag{8}$$

$$b(\mathbf{v},q) = -\int_\Omega q\nabla\cdot\mathbf{v}\,\mathrm{d}\Omega. \tag{9}$$

And a linear form:

$$(\mathbf{w},\mathbf{b}) = \int_\Omega \mathbf{w}\cdot\mathbf{b}\,\mathrm{d}\Omega. \tag{10}$$

Then we can rewrite (4) in a compact form.
Find $(\mathbf{v},p)\in\mathscr{S}\times\mathscr{Q}$, *such that for all* $(\mathbf{w},q)\in\mathscr{V}\times\mathscr{Q}$

$$\begin{aligned}&a(\mathbf{w},\mathbf{v}) + b(\mathbf{w},p) = (\mathbf{w},\mathbf{b}),\\ &b(\mathbf{v},q) = 0.\end{aligned} \tag{11}$$

We need to introduce the following space:

$$\mathscr{K} = \{\mathbf{v}\in\mathscr{V} | b(\mathbf{v},q) = 0\ \forall q\in\mathscr{Q}\}, \tag{12}$$

which is the space of divergence free velocities.

For (11) to have a unique solution, the following two conditions need to be satisfied:

$$a(v,v) \geqslant \alpha\|v\|_V^2 \quad \forall v\in\mathscr{K}, \tag{13}$$

$$\inf_{q\in\mathscr{Q}}\sup_{v\in\mathscr{V}}\frac{b(v,q)}{\|v\|_V\|q\|_Q} \geqslant \beta. \tag{14}$$

The first is known as the $\mathscr{K}$-coercivity condition and the second is known as the inf–sup or the LBB condition. They can be shown to hold for the continuous problem (11) [14]. In particular, the bilinear form $a(\cdot,\cdot)$ is coercive over the whole velocity space $\mathscr{V}$.

Now we consider the Galerkin approximation of (11), which reads:

Find $\mathbf{v}^h \in \mathscr{S}^h$ *and* $p^h \in \mathscr{Q}^h$, *such that for all* $(\mathbf{w}^h, q^h) \in \mathscr{V}^h \times \mathscr{Q}^h$

$$\begin{aligned} &a(\mathbf{w}^h, \mathbf{v}^h) + b(\mathbf{w}^h, p^h) = (\mathbf{w}^h, \mathbf{b}),\\ &b(\mathbf{v}^h, q^h) = 0, \end{aligned} \tag{15}$$

where $\mathscr{S}^h \in \mathscr{S}$, $\mathscr{Q}^h \in \mathscr{Q}$ and $\mathscr{V}^h \in \mathscr{V}$ are finite-dimensional spaces constructed via finite element procedures.

For (15) to have a unique a solution, the discrete counterparts of (13) and (14) are needed:

$$a(v_h, v_h) \geqslant \alpha \|v_h\|_V^2 \quad \forall v_h \in \mathscr{K}_h, \tag{16}$$

$$\inf_{q_h \in Q_h} \sup_{v_h \in V_h} \frac{b(v_h, q_h)}{\|v_h\|_V \|q_h\|_Q} \geqslant \beta, \tag{17}$$

where

$$\mathscr{K}_h = \{\mathbf{v}_h \in V_h | b(\mathbf{v}_h, q_h) = 0 \ \forall q_h \in Q_h\}. \tag{18}$$

The first condition holds since $a(\cdot,\cdot)$ is coercive on $\mathscr{V}$ and $\mathscr{K}_h \subset \mathscr{K} \subset \mathscr{V}$. But the second condition, known as the discrete inf–sup or the discrete LBB condition, does not hold automatically and needs to be checked for a particular FE approximation.

Before moving on, we first introduce some notations to represent the finite elements used. We denote by P_k if the unknown is approximated by complete polynomials of degree k. And we denote by Q_k the tensor product elements in which the unknown is approximated by k-degree polynomial along each dimension. Since we have both velocity and pressure as independent unknowns, an ordered pair will indicate the type of element. For example, the $Q1Q1$ element has bilinear velocity and bilinear pressure, while the $P1P0$ element has linear velocity and piecewise constant pressure. As we mentioned before, we will concentrate in this pare the low-order elements, i.e. $k < 2$. We are particularly interested in equal order elements, i.e. the $Q1Q1$ and $P1P1$ elements.

It is known [14] that the low-order elements do not satisfy the LBB condition. Since the low-order elements, especially the equal order elements are the most easily implemented in the practice, people proposed many procedures to deal with the problem of LBB condition. In general, they can be divided into two categories [15]:

- stable methods;
- stabilized methods.

The stable methods try to enrich the velocity space to satisfy the LBB condition. One example is the MINI element [16], which modifies the $P1P1$ element by adding a cubic bubble degree to the velocity. This internal degree is then eliminated from the weak form via a static condensation procedure.

The stabilized methods, on the other hand, coarsen the pressure space by modifying the original weak form. We are particularly interested in the Galerkin/Least-squares method, which considers the following functional.

$$L_s(\mathbf{w}, q) = (-\nu\nabla^2\mathbf{w} + \nabla q - \mathbf{b}, -\nu\nabla^2\mathbf{w} + \nabla q - \mathbf{b}), \tag{19}$$

which is the square of the residual of the strong form equation.

Take the first variation of (19) we obtain two equations:

$$(-\nu\nabla^2\mathbf{w}, -\nu\nabla^2\mathbf{v} + \nabla p - \mathbf{b}) = 0 \quad \forall \mathbf{w} \in \mathscr{V}, \tag{20}$$

$$(\nabla q, -\nu\nabla^2\mathbf{v} + \nabla p - \mathbf{b}) = 0 \quad \forall q \in \mathscr{Q}. \tag{21}$$

Obviously, the stationary point of (19) also solves the original problem (4). So we can add the above two equations to the original weak form without losing the consistency. Since we do not want additional continuity requirements, the above two equations are satisfied on the element interiors only, i.e. the jump terms along element edges are dropped. We will have the following modified equations:

$$\begin{aligned} &a(\mathbf{w}^h, \mathbf{v}^h) + b(\mathbf{w}^h, p^h)\\ &+ \sum_{e=1}^{n_{el}} \tau_e(-\nu\nabla^2\mathbf{w}^h, -\nu\nabla^2\mathbf{v}^h + \nabla p^h - \mathbf{b})_{\Omega^e} = (\mathbf{w}^h, \mathbf{b}),\\ &b(\mathbf{u}^h, q^h) - \sum_{e=1}^{n_{el}} \tau_e(\nabla q^h, -\nu\nabla^2\mathbf{v}^h + \nabla p^h - \mathbf{b})_{\Omega^e} = 0. \end{aligned} \tag{22}$$

In particular for low-order elements, the second derivatives of $\mathbf{v}$ will vanish. So the above equations reduce to

$$\begin{aligned} &a(\mathbf{w}^h, \mathbf{u}^h) + b(\mathbf{w}^h, p^h) = (\mathbf{w}^h, b),\\ &b(\mathbf{u}^h, q^h) - \sum_{e=1}^{n_{el}} \tau_e(\nabla q^h, \nabla p^h)_{\Omega^e} = -\sum_{e=1}^{n_{el}} \tau_e(\nabla q^h, \mathbf{b})_{\Omega^e}, \end{aligned} \tag{23}$$

where τ_e is the stabilization parameter. As we mentioned before, τ_e affects the computational results dearly and its exact value can only be determined empirically, i.e. from experiments or the corresponding 1-D problems. One such discussion can be found in [17]. For the Stokes problem, the parameter can be chosen as [18]

$$\tau_e = \frac{1}{3}\frac{h_e^2}{4\nu}, \tag{24}$$

where h_e is the characteristic element size. For a rigorous study of the convergence theory of the GLS method, please refer to [19].

3. The variational multiscale stabilized method formulation

3.1. The multiscale concept

We start from the original weak form (4). Consider the following decomposition:

$$\begin{aligned} &\mathbf{v} = \bar{\mathbf{v}} + \mathbf{v}', \qquad p = \bar{p} + p',\\ &\mathbf{w} = \bar{\mathbf{w}} + \mathbf{w}', \quad q = \bar{q} + q', \end{aligned} \tag{25}$$

where $\bar{\mathbf{v}}$, $\bar{\mathbf{w}}$, $\bar{p}$ and $\bar{q}$ represent the "coarse scale" functions, while $\mathbf{v}'$, $\mathbf{w}'$, p' and q' represent the "fine scale" functions. We can think the coarse scale functions as the ones obtained through an FE approximation, and the fine scale functions as the complement of their coarse scale part to the real solutions. Based on this idea, we can define the corresponding function spaces. Take the trial velocity function spaces as an example. The original space is decomposed as

$$\mathscr{S} = \bar{\mathscr{S}} \oplus \mathscr{S}' \tag{26}$$

and

$$\bar{\mathbf{v}} \in \bar{\mathscr{S}}, \quad \mathbf{v}' \in \mathscr{S}'. \tag{27}$$

The space $\bar{\mathscr{S}}$ is the finite-dimensional space obtained through an FE discretization, i.e. the $\mathscr{S}^h$ in (15) and $\mathscr{S}'$ is an infinite-dimensional space. Note that we require $\bar{\mathbf{v}}$ to satisfy the Dirichlet boundary conditions, i.e.:

$$\bar{\mathbf{v}} = \mathbf{v}^0 \quad \text{on } \Gamma. \tag{28}$$

Thus, $\mathbf{v}'$ equals zero on the boundary:

$$\mathbf{v}' = 0 \quad \text{on } \Gamma. \tag{29}$$

Substitute the decomposition into the original weak form (4), we will end up with two sub-problems:

$$\begin{aligned} &a(\bar{\mathbf{w}}, \bar{\mathbf{v}}) + a(\bar{\mathbf{w}}, \mathbf{v}') + b(\bar{\mathbf{w}}, \bar{p}) + b(\bar{\mathbf{w}}, p') = (\bar{\mathbf{w}}, \mathbf{b}), \\ &b(\bar{\mathbf{v}}, \bar{q}) + b(\mathbf{v}', \bar{q}) = 0, \end{aligned} \tag{30}$$

$$\begin{aligned} &a(\mathbf{w}', \bar{\mathbf{v}}) + a(\mathbf{w}', \mathbf{v}') + b(\mathbf{w}', \bar{p}) + b(\mathbf{w}', p') = (\mathbf{w}', \mathbf{b}), \\ &b(\bar{\mathbf{v}}, q') + b(\mathbf{v}', q') = 0. \end{aligned} \tag{31}$$

The first one is for the coarse scale and the second one is for the fine scale.

The idea of the variational multiscale method is to solve the fine scale problem analytically to express the fine scale solution $\mathbf{v}'$ and p' in terms of $\bar{\mathbf{v}}$ and $\bar{p}$, i.e.:

$$\mathbf{v}' = \mathbf{A} \cdot \bar{\mathbf{v}} + \mathbf{c}\bar{p}, \tag{32}$$

$$p' = \mathbf{d} \cdot \bar{\mathbf{v}} + e\bar{p}, \tag{33}$$

where $\mathbf{A}$, $\mathbf{c}$, $\mathbf{d}$ and e are to be determined. Once we have the fine scale solution, we can substitute them back into the coarse scale equations to obtain modified coarse scale equations expressed solely in coarse scale functions. We can then solve the modified coarse scale equations via FEM.

Before we move to the fine scale equations, we make a slight change to the coarse scale equations (30). Note we have the following identity:

$$\begin{aligned} b(\mathbf{v}', \bar{q}) &= -\int_\Omega \bar{q}(\nabla \cdot \mathbf{v}')\,\mathrm{d}\Omega \\ &= \int_\Omega (\nabla \bar{q} \cdot \mathbf{v}')\,\mathrm{d}\Omega - \int_\Gamma \bar{q}\mathbf{v}' \cdot \mathbf{n}\,\mathrm{d}\Gamma \\ &= \int_\Omega (\nabla \bar{q} \cdot \mathbf{v}')\,\mathrm{d}\Omega = b^*(\mathbf{v}', \bar{q}). \end{aligned} \tag{34}$$

So (30) can be changed to

$$\begin{aligned} &a(\bar{\mathbf{w}}, \bar{\mathbf{v}}) + a(\bar{\mathbf{w}}, \mathbf{v}') + b(\bar{\mathbf{w}}, \bar{p}) + b(\bar{\mathbf{w}}, p') = (\bar{\mathbf{w}}, \mathbf{b}), \\ &b(\bar{\mathbf{v}}, \bar{q}) + b^*(\mathbf{v}', \bar{q}) = 0. \end{aligned} \tag{35}$$

3.2. The fine scale solutions

In this section, we concentrate on the fine scale equations (31). Its strong form can be shown as the following equations:

$$\nabla \cdot \boldsymbol{\sigma}' + \nabla \cdot \bar{\boldsymbol{\sigma}} + \mathbf{b} = 0 \quad \text{in } \Omega, \tag{36}$$

$$\nabla \cdot \mathbf{v}' = -\nabla \cdot \bar{\mathbf{v}} \quad \text{in } \Omega, \tag{37}$$

$$\mathbf{v}' = 0 \quad \text{on } \Gamma, \tag{38}$$

where the Cauchy stress $\boldsymbol{\sigma}$ is defined as

$$\boldsymbol{\sigma} = v\nabla^s \mathbf{v} - p\mathbf{1}. \tag{39}$$

Now we make the approximation by viewing the fine scale problem as a Stokes problem, i.e.

$$\nabla \cdot \boldsymbol{\sigma}' + \bar{\mathbf{b}} = 0 \quad \text{in } \Omega, \tag{40}$$

$$\nabla \cdot \mathbf{v}' \approx 0 \quad \text{in } \Omega, \tag{41}$$

$$\mathbf{v}' = 0 \quad \text{on } \Gamma, \tag{42}$$

where

$$\bar{\mathbf{b}} = \nabla \cdot \bar{\boldsymbol{\sigma}} + \mathbf{b}. \tag{43}$$

Remark 3.1. $\bar{\mathbf{b}}$ is the coarse scale residual. So the fine scale solutions are driven by the coarse scale residual.

Ladyzhenskaya [20] showed that the solution of (40)–(42) can be expressed as follows:

$$\begin{aligned} v'_m(\mathbf{x}) = &\int_\Omega v^*_{mi}(\mathbf{x}-\mathbf{y})\bar{b}_i(\mathbf{y})\,\mathrm{d}\Omega_y - \int_{\partial\Omega} v^*_{mi}(\mathbf{x}-\mathbf{y})t'_i(\mathbf{y})\,\mathrm{d}S_y \\ &+ \int_{\partial\Omega} v'_i(\mathbf{x}-\mathbf{y})t^*_{mi}(\mathbf{y})\,\mathrm{d}S_y, \end{aligned} \tag{44}$$

$$\begin{aligned} p'(\mathbf{x}) = &\int_\Omega p^*_k(\mathbf{x}-\mathbf{y})\bar{b}_k(\mathbf{y})\,\mathrm{d}\Omega_y - \int_{\partial\Omega} p^*_k(\mathbf{x}-\mathbf{y})t'_k(\mathbf{y})\,\mathrm{d}S_y \\ &- 2v\int_{\partial\Omega} \frac{\partial p^*_k}{\partial x_i} v'_k n_i\,\mathrm{d}S_y, \end{aligned} \tag{45}$$

where $\mathbf{v}^*$ and p^* are Green's functions of the Stokes problem in an infinite domain. For the 2-D problem we have [21]

$$v^*_{ij}(\mathbf{x}, \mathbf{y}) = \frac{1}{4\pi v}\left(-\ln|\mathbf{x}-\mathbf{y}| + \frac{(x_i - y_i)(x_j - y_j)}{|\mathbf{x}-\mathbf{y}|^2}\right), \tag{46}$$

$$p^*_i(\mathbf{x}, \mathbf{y}) = \frac{(x_i - y_i)}{2\pi|\mathbf{x}-\mathbf{y}|^2}. \tag{47}$$

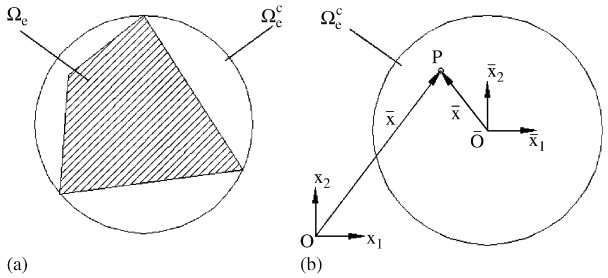

Fig. 1. The equivalent element domain: (a) Definition of Ω_e^c; (b) the local coordinate system.

Also in (44) and (45), the subindex y in $\mathrm{d}\Omega_y$ and $\mathrm{d}S_y$ means to integrate with respect to $\mathbf{y}$. t_{im}^* and t_i' are the traction obtained from Green's functions and fine scale solutions, respectively,

$$t_{im}^* = \sigma_{mij}' n_j = \left(\frac{v}{2}(v_{mi,j}' + v_{mj,i}') - p_m' \delta_{ij}\right) n_j, \tag{48}$$

$$t_i' = \sigma_{ij}' n_j = \left(\frac{v}{2}(v_{i,j}' + v_{j,i}') - p' \delta_{ij}\right) n_j. \tag{49}$$

In (44) and (45), the fine scale solutions are coupled with the coarse scale residual *globally*, i.e. the coarse scale residual at every point in Ω will contribute the fine scale solutions. From the perspective of FEM, we want the coupling effect to be limited within a local domain, so that the (modified) stiffness matrix will still be banded. In particular, we want the local domain to be associated with the finite element mesh. To this end, we consider a planar division of Ω, expressed as a set of elements $\{\Omega_e\}$, $e = 1 \ldots n_{el}$. For each element domain Ω_e, we now define an equivalent element domain Ω_e^c as the smallest circle enclosing Ω_e. Fig. 1(a) illustrates such an equivalent element domain associated with a quadrilateral element. And we can define a local coordinate system for each Ω_e^c, which is shown in Fig. 1(b). The local coordinate system $\bar{O} - \bar{x}_1 - \bar{x}_2$ has the origin at the center of Ω_e^c.

We shall now consider the local version of (44) and (45)

$$v_m'(\mathbf{x}) = \int_{\Omega_e^c} v_{mi}^*(\mathbf{x}-\mathbf{y})\bar{b}_i(\mathbf{y})\,\mathrm{d}\Omega_y - \int_{\partial\Omega_e^c} v_{mi}^*(\mathbf{x}-\mathbf{y})t_i'(\mathbf{y})\,\mathrm{d}S_y + \int_{\partial\Omega_e^c} v_i'(\mathbf{x}-\mathbf{y})t_{mi}^*(\mathbf{y})\,\mathrm{d}S_y, \tag{50}$$

$$p'(\mathbf{x}) = \int_{\Omega_e^c} p_k^*(\mathbf{x}-\mathbf{y})\bar{b}_k(\mathbf{y})\,\mathrm{d}\Omega_y - \int_{\partial\Omega_e^c} p_k^*(\mathbf{x}-\mathbf{y})t_k'(\mathbf{y})\,\mathrm{d}S_y - 2v\int_{\partial\Omega_e^c} \frac{\partial p_k^*}{\partial x_i} v_k' n_i\,\mathrm{d}S_y. \tag{51}$$

The above equations are for points $\mathbf{x} \in \Omega_e$.

Remark 3.2. Eqs. (50) and (51) are equivalent to (44) and (45). The contribution from outside Ω_e^c are now represented by the boundary integrals.

Now in order to limit the interaction between the two scales within the local domain Ω_e^c, we make the approximation by neglecting the boundary integral terms. Then (50) and (51) become

$$v_m'(\mathbf{x}) = \int_{\Omega_e^c} v_{mi}^*(\mathbf{x}-\mathbf{y})\bar{b}_i(\mathbf{y})\,\mathrm{d}\Omega_y, \tag{52}$$

$$p'(\mathbf{x}) = \int_{\Omega_e^c} p_k^*(\mathbf{x}-\mathbf{y})\bar{b}_k(\mathbf{y})\,\mathrm{d}\Omega_y \tag{53}$$

we also need the expression of the strain rate, which can be obtained from (52)

$$\frac{1}{2}\left(v_{m,j}'(\mathbf{x}) + v_{m,j}'(\mathbf{x})\right) = \int_{\Omega_e^c} \frac{1}{2}\left(v_{mi,j}^*(\mathbf{x}-\mathbf{y}) + v_{ji,m}^*(\mathbf{x}-\mathbf{y})\right)\bar{b}_i(\mathbf{y})\,\mathrm{d}\Omega_y. \tag{54}$$

Remark 3.3. The omittance of the outside contributions is the main approximation of the formulation. We actually approximate the infinite Green's functions as the element Green's functions. By making this approximation, the interaction between the two scales are confined within the equivalent element domain.

Eqs. (53)–(54) still cannot be evaluated, since the unknown coarse scale residual is inside the integral. We now consider the Taylor series expansion of the coarse scale residual $\bar{\mathbf{b}}(\mathbf{y})$ at the point $\mathbf{x}$:

$$\bar{\mathbf{b}}(\mathbf{y}) = \sum_{|\alpha|=0}^{\infty} \frac{1}{\alpha!} D^\alpha \bar{\mathbf{b}}(\mathbf{x})(\mathbf{x}-\mathbf{y})^\alpha, \tag{55}$$

where $\alpha = (\alpha_1, \ldots, \alpha_d)$ is a d-dimensional multiindex. We will only keep the constant term

$$\bar{\mathbf{b}}(\mathbf{y}) \approx \bar{\mathbf{b}}(\mathbf{x}). \tag{56}$$

Then the Eqs. (52)–(54) become

$$v_m'(\mathbf{x}) = \int_{\Omega_e^c} v_{mi}^*(\mathbf{x}-\mathbf{y})\,\mathrm{d}\Omega_y \bar{b}_i(\mathbf{x}), \tag{57}$$

$$p'(\mathbf{x}) = \int_{\Omega_e^c} p_k^*(\mathbf{x}-\mathbf{y})\,\mathrm{d}\Omega_y \bar{b}_k(\mathbf{x}), \tag{58}$$

$$\frac{1}{2}(v_{m,j}'(\mathbf{x}) + v_{m,j}'(\mathbf{x})) = \int_{\Omega_e^c} \frac{1}{2}\left(v_{mi,j}^*(\mathbf{x}-\mathbf{y}) + v_{ji,m}^*(\mathbf{x}-\mathbf{y})\right)\mathrm{d}\Omega_y \bar{b}_i(\mathbf{x}). \tag{59}$$

Remark 3.4. By the approximation (56), we assume that the coarse scale residual is constant within Ω_e^c. Of course, this is only true when the mesh size approaches zero.

We can write (58)–(59) in a compact form

$$\mathbf{v}' = \mathbf{T} \cdot [\nabla \cdot (v \nabla^s \bar{\mathbf{v}}) - \nabla \bar{p} + \mathbf{b}], \tag{60}$$

$$\nabla^s \mathbf{v}' = \mathbf{F} \cdot [\nabla \cdot (v \nabla^s \bar{\mathbf{v}}) - \nabla \bar{p} + \mathbf{b}], \tag{61}$$

$$p' = \mathbf{e} \cdot [\nabla \cdot (v : \nabla^s \bar{\mathbf{v}}) - \nabla \bar{p} + \mathbf{b}]. \tag{62}$$

The vector $\mathbf{e}$, second order tensor $\mathbf{T}$ and third order tensor $\mathbf{F}$ have the following expressions:

$$e_k = \int_{\Omega_e^c} p_k^*(\mathbf{x} - \mathbf{y}) \, \mathrm{d}\Omega_y, \tag{63}$$

$$T_{mi} = \int_{\Omega_e^c} v_{mi}^*(\mathbf{x} - \mathbf{y}) \, \mathrm{d}\Omega_y, \tag{64}$$

$$F_{imn} = \int_{\Omega_e^c} \frac{1}{2}(v_{im,n}^*(\mathbf{x} - \mathbf{y}) + v_{in,m}^*(\mathbf{x} - \mathbf{y})) \, \mathrm{d}\Omega_y. \tag{65}$$

We can obtain closed-form expressions for them. The detailed derivations are in the Appendix and the results are

$$e_k = -\frac{\bar{x}_k}{2}, \tag{66}$$

$$T_{mi} = \left[\frac{1}{4v} a^2 (1 - \ln a) - \frac{3}{16v} |\bar{\mathbf{x}}|^2\right] \delta_{im} + \frac{1}{8v} \bar{x}_i \bar{x}_m, \tag{67}$$

$$F_{imn} = \frac{1}{8v} [\delta_{ij} \bar{x}_m - (\delta_{jm} \bar{x}_i + \delta_{im} \bar{x}_j)], \tag{68}$$

where a is the radius of Ω_e^c and $\bar{\mathbf{x}}$ is the local coordinate of the point $\mathbf{x}$.

Since we are dealing with low-order elements, Eqs. (60)–(62) reduce to

$$\mathbf{v}' = \mathbf{T} \cdot [-\nabla \bar{p} + \mathbf{b}], \tag{69}$$

$$\nabla^s \mathbf{v}' = \mathbf{F} \cdot [-\nabla \bar{p} + \mathbf{b}], \tag{70}$$

$$p' = \mathbf{e} \cdot [-\nabla \bar{p} + \mathbf{b}]. \tag{71}$$

These are the final expressions of the fine scale equations.

3.3. The modified coarse scale equations and FE implementation

Substitute (69)–(71) into the coarse scale equations (35), we get the modified coarse scale equations

$$\begin{aligned} &\int_{\Omega_e} \nabla^s \bar{\mathbf{w}}^h : v \nabla^s \bar{\mathbf{v}}^h \, \mathrm{d}\Omega - \int_{\Omega_e} \nabla^s \bar{\mathbf{w}}^h : v\mathbf{F} \cdot \nabla \bar{p}^h \, \mathrm{d}\Omega \\ &\quad - \int_{\Omega_e} \left(\nabla \cdot \bar{\mathbf{w}}^h \bar{p}^h - \mathbf{e} \cdot \nabla \bar{p}^h\right) \mathrm{d}\Omega \\ &\qquad = \int_{\Omega_e} \bar{\mathbf{w}}^h \cdot \mathbf{b} \, \mathrm{d}\Omega - \int_{\Omega_e} \nabla^s \bar{\mathbf{w}}^h : v\mathbf{F} \cdot \mathbf{b} \, \mathrm{d}\Omega \\ &\qquad\quad + \int_{\Omega_e} \nabla \cdot \bar{\mathbf{w}}^h (\mathbf{e} \cdot \mathbf{b}) \, \mathrm{d}\Omega, \end{aligned} \tag{72}$$

$$\begin{aligned} &- \int_{\Omega_e} \bar{q}^h \nabla^s \mathbf{v}^h \, \mathrm{d}\Omega - \int_{\Omega_e} \nabla \bar{q}^h \cdot \mathbf{T} \cdot \nabla \bar{p}^h \, \mathrm{d}\Omega \\ &\quad = - \int_{\Omega_e} \nabla \bar{q}^h \cdot \mathbf{T} \cdot \mathbf{b} \, \mathrm{d}\Omega. \end{aligned} \tag{73}$$

Both equations are now in terms of the coarse scale functions $\bar{\mathbf{v}}^h$, $\bar{\mathbf{w}}^h$, $\bar{p}^h$ and $\bar{q}^h$. We can apply the standard FE procedures.

Consider the following velocity approximation:

$$\mathbf{v}^h = \mathbf{u}^h + \mathbf{v}_0^h, \tag{74}$$

where $\mathbf{u}^h \in \mathscr{V}^h$ and $\mathbf{v}_0^h$ satisfies the essential boundary conditions. They have the following expressions:

$$\mathbf{u}^h(\mathbf{x}) = \sum_{A \in \eta \setminus \eta_v} \mathbf{N}_A(\mathbf{x}) \mathbf{u}_A, \tag{75}$$

$$\mathbf{v}_0^h(\mathbf{x}) = \sum_{A \in \eta_v} \mathbf{N}_A(\mathbf{x}) \mathbf{v}^0(\mathbf{x}_A), \tag{76}$$

$$\mathbf{w}^h(\mathbf{x}) = \sum_{A \in \eta \setminus \eta_v} \mathbf{N}_A(\mathbf{x}) \mathbf{w}_A, \tag{77}$$

where $\mathbf{N}_A$ are the velocity shape functions and

$\eta = \{\text{All Velocity Node Numbers}\}$,

$\eta_v = \{\text{Velocity Node Numbers Corresponding to } \Gamma_v\}$.

The approximated pressure field is

$$p^h = \sum_{A \in \hat{\eta}} M_A(\mathbf{x}) p_A, \tag{78}$$

$$q^h = \sum_{A \in \hat{\eta}} M_A(\mathbf{x}) q_A, \tag{79}$$

where $\mathbf{M}_A$ are the pressure shape functions and $\hat{\eta}$ is the set of pressure node numbers.

Then Eqs. (72) and (73) can be written in a matrix form

$$\begin{pmatrix} \bar{\mathbf{K}} & \bar{\mathbf{G}} \\ \bar{\mathbf{L}} & \bar{\mathbf{E}} \end{pmatrix} \begin{pmatrix} \bar{\mathbf{u}} \\ \bar{\mathbf{p}} \end{pmatrix} = \begin{pmatrix} \bar{\mathbf{f}} \\ \bar{\mathbf{h}} \end{pmatrix}, \tag{80}$$

where

$$\bar{\mathbf{K}} = \mathop{\mathbf{A}}_{e=1}^{n_{el}} \bar{\mathbf{K}}_e, \tag{81}$$

$$\bar{\mathbf{G}} = \mathop{\mathbf{A}}_{e=1}^{n_{el}} \bar{\mathbf{G}}_e, \tag{82}$$

$$\bar{\mathbf{L}} = \mathop{\mathbf{A}}_{e=1}^{n_{el}} \bar{\mathbf{L}}_e, \tag{83}$$

$$\bar{\mathbf{E}} = \mathop{\mathbf{A}}_{e=1}^{n_{el}} \bar{\mathbf{E}}_e, \tag{84}$$

$$\bar{\mathbf{f}} = \mathop{\mathbf{A}}_{e=1}^{n_{el}} \bar{\mathbf{f}}_e, \tag{85}$$

$$\bar{\mathbf{h}} = \mathop{\mathbf{A}}_{e=1}^{n_{el}} \bar{\mathbf{h}}_e. \tag{86}$$

The element matrices and element vectors have the following expressions:

$$\bar{\mathbf{K}}_e = \int_{\Omega_e} \mathbf{B}_v^{eT} \mathbf{C} \mathbf{B}_v^e \, d\Omega, \tag{87}$$

$$\bar{\mathbf{G}}_e = -\int_{\Omega_e} \mathbf{B}_v^{eT} [\mathbf{d}(\mathbf{N}_p^e - \mathbf{e}^T \mathbf{B}_p^e) + \mathbf{C}\mathbf{F}\mathbf{B}_p^e] \, d\Omega, \tag{88}$$

$$\bar{\mathbf{L}}_e = -\int_{\Omega_e} \mathbf{N}_p^{eT} \mathbf{d}^T \mathbf{B}_v^e \, d\Omega, \tag{89}$$

$$\bar{\mathbf{E}}_e = -\int_{\Omega_e} \mathbf{B}_p^T \mathbf{T} \mathbf{B}_p^e \, d\Omega, \tag{90}$$

$$\bar{\mathbf{f}}_e = \int_{\Omega_e} [\mathbf{N}_v^{eT} + \mathbf{B}_v^{eT}(\mathbf{d}\mathbf{e}^T - \mathbf{C}\mathbf{F})] \mathbf{b}^e \, d\Omega - \int_{\Omega_e} \mathbf{B}_v^{eT} \mathbf{C} \mathbf{B}_v^e \, d\Omega \bar{\mathbf{v}}^{0e}, \tag{91}$$

$$\bar{\mathbf{h}}_e = -\int_{\Omega_e} \mathbf{B}_p^{eT} \mathbf{T} \mathbf{b}^e \, d\Omega + \int_{\Omega_e} \mathbf{N}_p^{eT} \mathbf{B}_v^e \, d\Omega \bar{\mathbf{v}}^{0e}. \tag{92}$$

The vector $\bar{\mathbf{v}}^{0e}$ equals zero for interior nodes. For all the matrices and vectors involved, $\mathbf{N}_v^e$ and $\mathbf{B}_v^e$ are the shape functions matrix and shape function derivatives matrix for the velocity:

$$\mathbf{N}_v^e = \begin{bmatrix} N_1^e(\mathbf{x}) & 0 & N_2^e(\mathbf{x}) & 0 & \cdots\cdots & N_{n_{ed}^v}^e(\mathbf{x}) & 0 \\ 0 & N_1^e(\mathbf{x}) & 0 & N_2^e(\mathbf{x}) & \cdots\cdots & 0 & N_{n_{ed}^v}^e(\mathbf{x}) \end{bmatrix}, \tag{93}$$

$$\mathbf{B}_v^e = \begin{bmatrix} N_{1,x}^e(\mathbf{x}) & 0 & N_{2,x}^e(\mathbf{x}) & 0 & \cdots\cdots & N_{n_{ed}^v,x}^e(\mathbf{x}) & 0 \\ 0 & N_{1,y}^e(\mathbf{x}) & 0 & N_{2,y}^e(\mathbf{x}) & \cdots\cdots & 0 & N_{n_{ed}^v,y}^e(\mathbf{x}) \\ N_{1,y}^e(\mathbf{x}) & N_{2,x}^e(\mathbf{x}) & N_{2,y}^e(\mathbf{x}) & N_{2,x}^e(\mathbf{x}) & \cdots\cdots & N_{n_{ed}^v,y}^e(\mathbf{x}) & N_{n_{ed}^v,x}^e(\mathbf{x}), \end{bmatrix}, \tag{94}$$

where n_{ed}^v is the number of velocity nodes per element. $\mathbf{N}_p^e$ and $\mathbf{B}_p^e$ are the shape functions matrix and shape function derivatives matrix for the pressure

$$\mathbf{N}_p^e = [M_1^e(\mathbf{x}) \;\; M_2^e(\mathbf{x}) \;\; \cdots\cdots \;\; M_{n_{ed}^v}^e(\mathbf{x})], \tag{95}$$

$$\mathbf{B}_p^e = \begin{bmatrix} M_{1,x}^e(\mathbf{x}) & M_{2,x}^e(\mathbf{x}) & \cdots\cdots & M_{n_{ed}^v,x}^e(\mathbf{x}) \\ M_{1,y}^e(\mathbf{x}) & M_{2,y}^e(\mathbf{x}) & \cdots\cdots & M_{n_{ed}^v,y}^e(\mathbf{x}) \end{bmatrix}. \tag{96}$$

The matrix form of the tensors $\mathbf{C}$, $\mathbf{F}$, $\mathbf{T}$ and the vector $\mathbf{e}$ are

$$\mathbf{C} = \begin{bmatrix} 2\nu & 0 & 0 \\ 0 & 2\nu & 0 \\ 0 & 0 & \nu \end{bmatrix}, \tag{97}$$

$$\mathbf{F} = \frac{1}{8\nu} \begin{bmatrix} -\bar{x}_1 & \bar{x}_2 \\ \bar{x}_1 & -\bar{x}_2 \\ -\bar{x}_2 & \bar{x}_1 \end{bmatrix}, \tag{98}$$

$$\mathbf{T} = \begin{bmatrix} c + \frac{1}{8\nu}\bar{x}_1^2 & \frac{1}{8\nu}\bar{x}_1\bar{x}_2 \\ \frac{1}{8\nu}\bar{x}_1\bar{x}_2 & c + \frac{1}{8\nu}\bar{x}_2^2 \end{bmatrix}, \tag{99}$$

$$\mathbf{e} = \frac{1}{2} \begin{bmatrix} -\bar{x}_1 \\ -\bar{x}_2 \end{bmatrix}, \tag{100}$$

where

$$c = \frac{1}{4\nu} a^2 (1 - \ln a) - \frac{3}{16\nu} |\bar{\mathbf{x}}|^2. \tag{101}$$

The $\mathbf{d}$ vector is used to get the divergence term:

$$\mathbf{d} = \begin{bmatrix} 1 \\ 1 \\ 0 \end{bmatrix}. \tag{102}$$

The system (103) can then be solved to get the solution.

Remark 3.5. The coefficient matrix of (103) is not symmetric in general. But in the linear triangle case, we will use 1-point numerical quadrature. And the quadrature point will be the same as the origin of the local coordinate system. Then $\bar{\mathbf{x}} = \mathbf{0}$. In this case we will have

$$\begin{pmatrix} \mathbf{K} & \mathbf{G}^T \\ \mathbf{G} & \bar{\mathbf{E}} \end{pmatrix} \begin{pmatrix} \bar{\mathbf{u}} \\ \bar{\mathbf{p}} \end{pmatrix} = \begin{pmatrix} \mathbf{f} \\ \bar{\mathbf{h}} \end{pmatrix}, \tag{103}$$

where the $\bar{\mathbf{E}}$ matrix will be of the same form as the one obtained from the GLS method, with the stabilization parameter:

$$\tau_e = \frac{1}{4\nu} a^2 (1 - \ln a). \tag{104}$$

Remark 3.6. Compared to the GLS method, we can see the matrix $\mathbf{T}$ acting as the stabilization parameter matrix. From the derivation we know the stabilized term is due to the interaction between the two scales, in particular (69).

4. Numerical results

In this section we compute two numerical examples to illustrate the performance of the proposed VMS method. As we mentioned in the beginning, the pressure for the pure Dirichlet problem can only be determined up to a constant. To remove the spurious constant pressure modes, for both examples we prescribe $p = 0$ at the point $(0, 0)$.

4.1. Analytical Stokes

The first example [18] is used to show the convergence of the proposed VMS method. We consider a square domain $\Omega = [0, 1] \times [0, 1]$ with zero boundary condition. ν is taken as 1 and

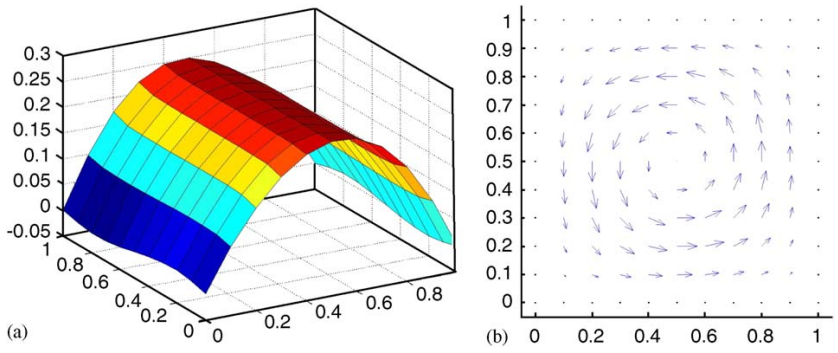

Fig. 2. The analytical Stokes problem: (a) Pressure plots; (b) velocity plots.

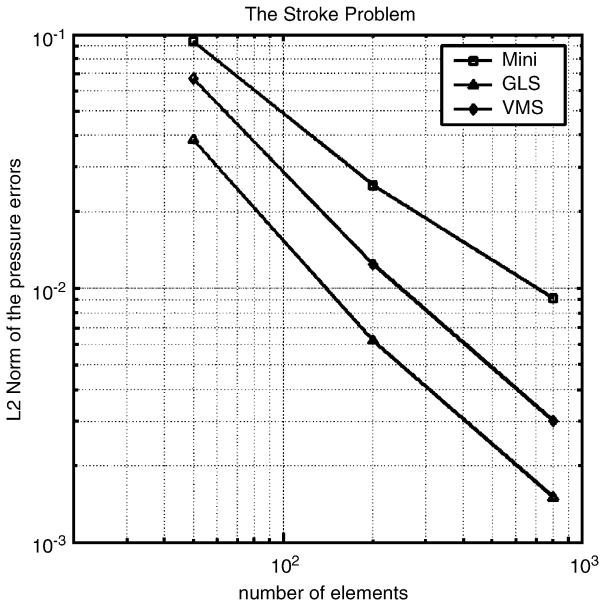

Fig. 3. Convergence plot.

the components of the body force **b** are

$$b_1 = (12 - 24y)x^4 + (-24 + 48y)x^3 + (-48y + 72y^2 - 48y^3 + 12)x^2 + (-2 + 24y - 72y^2 + 48y^3)x + 1 - 4y + 12y^2 - 8y^3, \quad (105)$$

$$b_2 = (8 - 48y + 48y^2)x^3 + (-12 + 72y - 72y^2)x^2 + (4 - 24y + 48y^2 - 48y^3 + 24y^4)x - 12y^2 + 24y^3 - 12y^4. \quad (106)$$

In this case, the problem has a closed-form analytical solution

$$v_1 = x^2(1 - x)^2(2y - 6y^2 + 4y^3), \quad (107)$$

$$v_2 = -y^2(1 - y)^2(2x - 6x^2 + 4x^3), \quad (108)$$

$$p = x(1 - x). \quad (109)$$

We first calculate the problem by using the VMS method with 10×10 $Q1Q1$ elements. The velocity and pressure plots are shown in Fig. 2. We can observe that the VMS method gives stable pressure results.

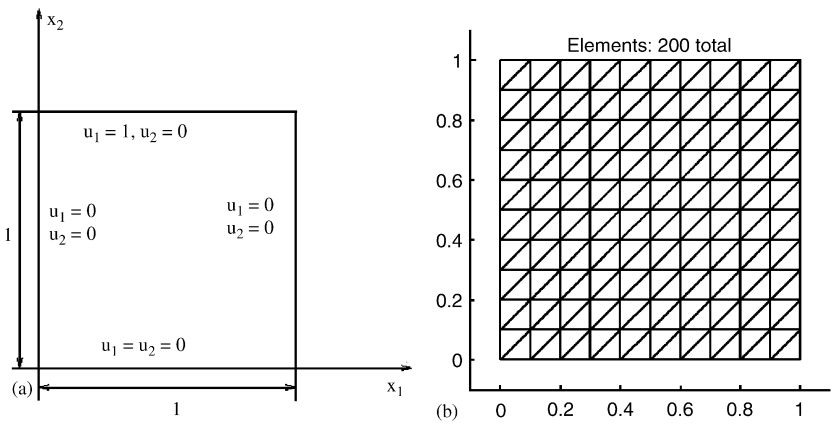

Fig. 4. The cavity problem: (a) The problem; (b) a sample mesh with triangle elements.

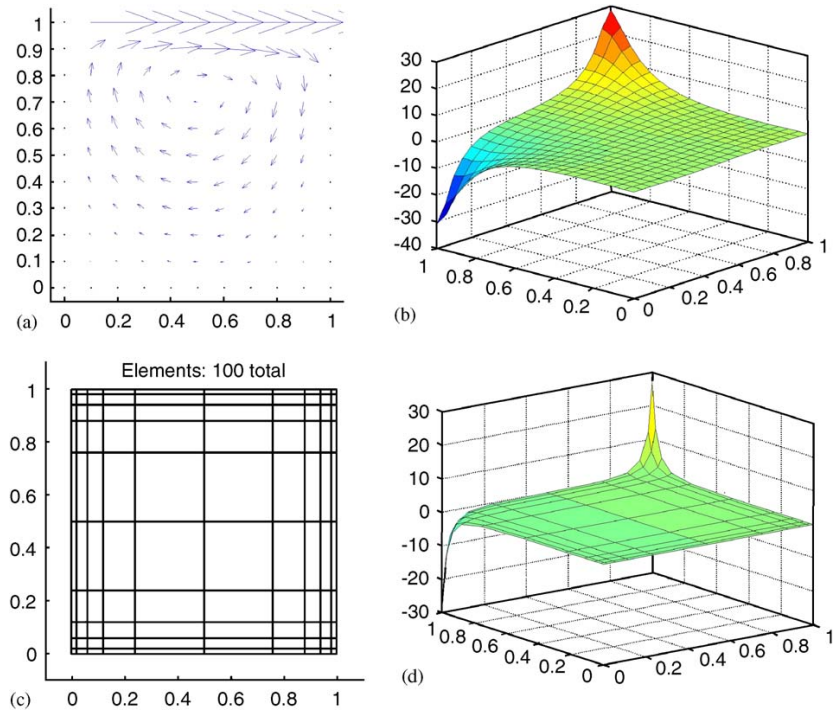

Fig. 5. The cavity problem: (a) Velocity plot for the VMS $P1P1$ element; (b) pressure plot for the $P1P1$ element; (c) a sample mesh with quadrilateral elements; (d) pressure plot for the VMS $Q1Q1$ element.

To study the convergence, we compute the problem with a series of meshes. Fig. 3 shows the plot of the $L2$ norm of theb error of the pressure against number of elements. We can see that the VMS method shows a similar convergence rate as the MINI element and the GLS element.

4.2. The lid-driven cavity problem

The cavity problem is a standard benchmark test for incompressible flows. It models a plane flow in a square lid-driven cavity. There is no body force. The upper side of the cavity moves at unit speed, while other sides are fixed. The problem definition is shown in Fig. 4(a).

The characteristics of this problem is the pressure singularities at both corners. We compute this problem with both the VMS $P1P1$ element and the VMS $Q1Q1$ element. The results are shown in Fig. 5. Again, the VMS method gives stable pressure result.

5. Conclusion

A stabilized method based on the variational multiscale formulation has been presented. The new method uses the infinite Green's functions to compute the fine scale solutions. By using special integration techniques, we are able to obtain an explicit expression of the local coupling effect between the two scales. Several approximations are also made and the most important one is to neglect the fine scale solutions on the element boundaries. The method follows solid variational formulations and produce a stabilized term similar to the one in the GLS formulation. The numerical results show that the proposed method can stabilize both $Q1Q1$ and $P1P1$ elements and has a good convergence rate.

The future work is to extend the approach to the general incompressible flow problem and the multidimensional advection–diffusion-reaction problem. In those cases, the issue of stabilizing the convective effects will be of interest. Also we are working on how to address the approximations we made during the derivation.

Acknowledgements

This work is made possible by an NSF grant (Grant No. CMS-0239130 to University of California at Berkeley), which is greatly appreciated.

Appendix

In this part, we show the detailed procedures in evaluating the integrals (63)–(65). We first make a coordinate transformation by changing the global coordinate $\mathbf{x}$ and $\mathbf{y}$ to the local coordinate $\bar{\mathbf{x}}$ and $\bar{\mathbf{y}}$. Note that the two coordinate system is different only by a translation, i.e.

$$\mathbf{x} = \bar{\mathbf{x}} + \mathbf{x}_c, \tag{110}$$

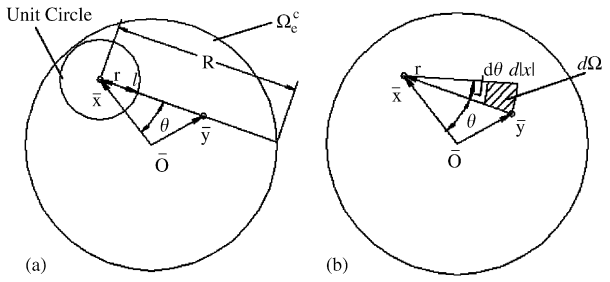

Fig. 6. Integration by using $d\Omega = |\mathbf{r}|\, d|\mathbf{r}|\, d\theta$: (a) Local coordinate system; (b) microarea element.

where $\mathbf{x}_c$ is the global coordinate of the local origin. So we have

$$\mathbf{x} - \mathbf{y} = \bar{\mathbf{x}} - \bar{\mathbf{y}}, \quad d\Omega_{\mathbf{y}} = d\Omega_{\bar{\mathbf{y}}}.$$

So we can rewrite (63)–(65) as follows:

$$e_k = \int_{\Omega_e^c} p_k^*(\bar{\mathbf{x}} - \bar{\mathbf{y}})\, d\Omega_{\bar{y}}, \tag{111}$$

$$T_{mi} = \int_{\Omega_e^c} v_{mi}^*(\bar{\mathbf{x}} - \bar{\mathbf{y}})\, d\Omega_{\bar{y}}, \tag{112}$$

$$F_{imn} = \int_{\Omega_e^c} \frac{1}{2}(v_{im,n}^*(\bar{\mathbf{x}} - \bar{\mathbf{y}}) + v_{in,m}^*(\bar{\mathbf{x}} - \bar{\mathbf{y}}))\, d\Omega_{\bar{y}}. \tag{113}$$

We start with the **T** tensor. The expression of 2-D Green's function v_{mi}^* in the local coordinate system is

$$v_{mi}^*(\bar{\mathbf{x}}, \bar{\mathbf{y}}) = \frac{1}{4\pi v}\left(-\ln|\bar{\mathbf{x}} - \bar{\mathbf{y}}| + \frac{(\bar{x}_i - \bar{y}_i)(\bar{x}_m - \bar{y}_m)}{|\bar{\mathbf{x}} - \bar{\mathbf{y}}|^2}\right). \tag{114}$$

Now (112) becomes

$$\int_{\Omega_e^c} v_{mi}^*(\bar{\mathbf{x}} - \bar{\mathbf{y}})\, d\Omega_{\bar{y}} = \frac{1}{4\pi v}\int_{\Omega_e^c}\left(\frac{(\bar{x}_i - \bar{y}_i)(\bar{x}_m - \bar{y}_m)}{|\bar{\mathbf{x}} - \bar{\mathbf{y}}|^2} - \ln|\bar{\mathbf{x}} - \bar{\mathbf{y}}|\delta_{im}\right) d\Omega_{\bar{y}}. \tag{115}$$

So we need to evaluate the following two integrals:

$$\int_{\Omega_e^c} \frac{(\bar{x}_i - \bar{y}_i)(\bar{x}_m - \bar{y}_m)}{|\bar{\mathbf{x}} - \bar{\mathbf{y}}|^2}\, d\Omega_{\bar{y}}, \quad \int_{\Omega_e^c} \ln|\bar{\mathbf{x}} - \bar{\mathbf{y}}|\, d\Omega_{\bar{y}}.$$

We look at the two integrals separately. For the first integral, we express the microarea element $d\Omega$ as

$$d\Omega = |\mathbf{r}|\, d|\mathbf{r}|\, d\theta, \tag{116}$$

where $\mathbf{r} = \mathbf{x} - \mathbf{y}$. $|\mathbf{r}|$ goes from zero to R, which can be solved. Now we define

$$\ell_i = -\frac{r_i}{|\mathbf{r}|}. \tag{117}$$

Then ℓ_i is independent of $\mathbf{r}$. Please refer to Fig. 6.

Now we can write the first integral as

$$\int_{\Omega_e^c} \frac{r_i r_m}{|\mathbf{r}|^2}\, d\Omega = \int_{\Omega_e^c} \ell_i \ell_m\, d\Omega = \int_0^{2\pi}\int_0^{R(\ell)} \ell_i \ell_j \mathbf{r}\, d|\mathbf{r}|\, d\theta = \int_0^{2\pi} \frac{1}{2}\ell_i \ell_m R^2(\ell)\, d\theta. \tag{118}$$

R can be solved as

$$R = -f \pm \sqrt{f^2 + e}, \tag{119}$$

with

$$f = \ell_i \bar{x}_i, \quad e = a^2 - |\bar{\mathbf{x}}|^2.$$

Without losing the generality, we pick $R = -f - \sqrt{f^2 + e}$. Then

$$R^2 = 2f^2 + e + 2f\sqrt{f^2 + e}, \tag{120}$$

$$\int_{\Omega_e^c} \frac{r_i r_m}{|\mathbf{r}|^2}\, d\Omega = \int_0^{2\pi} \frac{1}{2}\ell_i \ell_m (2f^2 + e + 2f\sqrt{f^2 + e})\, d\theta. \tag{121}$$

The term $\ell_i \ell_m f\sqrt{f^2 + e}$ is odd in ℓ_i, so

$$\int_0^{2\pi} \ell_i \ell_m f\sqrt{f^2 + e} = 0. \tag{122}$$

Now the integral can be simplified

$$\int_{\Omega_e^c} \frac{r_i r_m}{|\mathbf{r}|^2}\, d\Omega = \int_0^{2\pi} \frac{1}{2}\ell_i \ell_m (2f^2 + e)\, d\theta = \int_0^{2\pi} (\ell_i \ell_m \ell_k \ell_\ell \bar{x}_k \bar{x}_\ell + e\ell_i \ell_m)\, d\theta. \tag{123}$$

Exploit the identities [22]

$$\int_0^{2\pi} \ell_i \ell_j\, d\theta = \pi\delta_{ij}, \tag{124}$$

$$\int_0^{2\pi} \ell_i \ell_j \ell_k \ell_\ell = \frac{\pi}{4}(\delta_{ij}\delta_{k\ell} + \delta_{ik}\delta_{j\ell} + \delta_{i\ell}\delta_{jk}). \tag{125}$$

We have

$$\begin{aligned}\int_{\Omega_e^c} \frac{r_i r_m}{|\mathbf{r}|^2}\, d\Omega &= \frac{1}{2}\pi e\delta_{im} + \frac{1}{4}\pi\bar{x}_k\bar{x}_\ell(\delta_{ij}\delta_{k\ell} + \delta_{ik}\delta_{j\ell} + \delta_{i\ell}\delta_{jk}) \\ &= \frac{\pi}{2}\delta_{im}(a^2 - \bar{x}_k\bar{x}_k) + \frac{\pi}{4}\bar{x}_k\bar{x}_k\delta_{im} + \frac{\pi}{2}\bar{x}_i\bar{x}_m \\ &= \frac{\pi}{2}\bar{x}_i\bar{x}_m + \frac{\pi}{2}a^2\delta_{im} - \frac{\pi}{4}|\bar{\mathbf{x}}|^2\delta_{im}.\end{aligned} \tag{126}$$

Now we look at the second integral

$$\int_{\Omega_e^c} \ln|\mathbf{r}|\, d\Omega.$$

The microarea element

$$d\Omega = |\bar{\mathbf{y}}|\, d|\bar{\mathbf{y}}|\, d\phi. \tag{127}$$

Here $|\bar{\mathbf{y}}|$ goes from 0 to a. Please refer to Fig. 7.

Exploit the cosine law

$$|\mathbf{r}| = \sqrt{|\mathbf{x}|^2 + |\mathbf{y}|^2 - 2|\mathbf{x}||\mathbf{y}|\cos\phi}. \tag{128}$$

Since $|\bar{\mathbf{x}}|$ is constant, we pull it outside the square root. Also we define $t = |\mathbf{y}|/|\mathbf{x}|$:

$$|\mathbf{r}| = |\bar{\mathbf{x}}|\sqrt{1 + t^2 - 2t\cos\phi}. \tag{129}$$

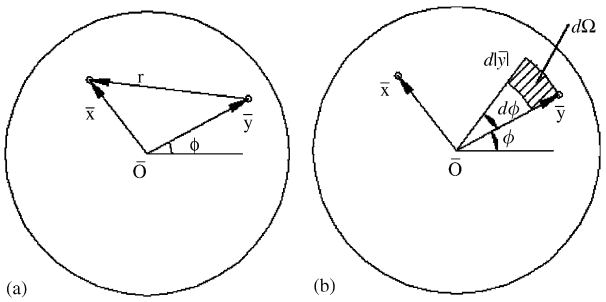

Fig. 7. Integration by using $d\Omega = |\bar{\mathbf{y}}|\, d|\bar{\mathbf{y}}|\, d\phi$: (a) Local coordinate system; (b) microarea element.

So,

$$\int_{\Omega_e^c} \ln|\mathbf{r}|\, d\Omega = \int_{\Omega_e^c} \ln|\bar{\mathbf{x}}|\, d\Omega + \frac{1}{2}\int_{\Omega_e^c} \ln(1+t^2-2t\cos\phi)\, d\Omega. \tag{130}$$

Look at the two terms separately

$$\int_{\Omega_e^c} \ln|\bar{\mathbf{x}}|\, d\Omega = \int_0^a |\bar{\mathbf{y}}|\, d|\bar{\mathbf{y}}| \int_0^{2\pi} (\ln|\bar{\mathbf{x}}|)\, d\phi = 2\pi \ln|\bar{\mathbf{x}}| \int_0^a |\bar{\mathbf{y}}|\, d|\bar{\mathbf{y}}| = \pi a^2 \ln|\bar{\mathbf{x}}|. \tag{131}$$

The other term

$$\frac{1}{2}\int_{\Omega_e^c} \ln(1+t^2-2t\cos\phi)\, d\Omega = \frac{1}{2}\int_0^a |\bar{\mathbf{y}}|\, d|\bar{\mathbf{y}}| \int_0^{2\pi} \ln(1+t^2-2t\cos\phi)\, d\phi. \tag{132}$$

We can evaluate the second integral of RHS [23]:

$$\int_0^{2\pi} \ln(1+t^2-2t\cos\phi)\, d\phi = \begin{cases} 0 & t \leqslant 1, \\ 2\pi \ln(t^2) & t \geqslant 1. \end{cases} \tag{133}$$

Since $|\bar{\mathbf{x}}| \leqslant a$ we need to break the integral into two parts: $0 \to |\bar{\mathbf{x}}|$ and $|\bar{\mathbf{x}}| \to a$:

$$\begin{aligned} &\frac{1}{2}\int_{\Omega_e^c} \ln(1+t^2-2t\cos\phi)\, d\Omega \\ &= \frac{1}{2}\int_0^{|\bar{\mathbf{x}}|} |\bar{\mathbf{y}}|\, d|\bar{\mathbf{y}}| \int_0^{2\pi} \ln(1+t^2-2t\cos\phi)\, d\phi \\ &\quad + \frac{1}{2}\int_{|\bar{\mathbf{x}}|}^a |\bar{\mathbf{y}}|\, d|\bar{\mathbf{y}}| \int_0^{2\pi} \ln(1+t^2-2t\cos\phi)\, d\phi \\ &= \frac{1}{2}\int_{|\bar{\mathbf{x}}|}^a |\bar{\mathbf{y}}|\, d|\bar{\mathbf{y}}| \int_0^{2\pi} \ln(1+t^2-2t\cos\phi)\, d\phi \\ &= \pi \int_{|\bar{\mathbf{x}}|}^a \ln(t^2) |\bar{\mathbf{y}}|\, d|\bar{\mathbf{y}}| \\ &= 2\pi \int_{|\bar{\mathbf{x}}|}^a (\ln|\bar{\mathbf{y}}| - \ln|\bar{\mathbf{x}}|) |\bar{\mathbf{y}}|\, d|\bar{\mathbf{y}}|. \end{aligned} \tag{134}$$

The two terms

$$\int_{|\bar{\mathbf{x}}|}^a (\ln|\bar{\mathbf{x}}|) |\bar{\mathbf{y}}|\, d|\bar{\mathbf{y}}| = \frac{1}{2}\ln|\bar{\mathbf{x}}| (a^2 - |\bar{\mathbf{x}}|^2) \tag{135}$$

$$\begin{aligned} &\int_{|\bar{\mathbf{x}}|}^a (\ln|\bar{\mathbf{y}}|) |\bar{\mathbf{y}}|\, d|\bar{\mathbf{y}}| \\ &= a^2\left(\frac{1}{2}\ln a - \frac{1}{4}\right) - |\bar{\mathbf{x}}|^2\left(\frac{1}{2}\ln|\bar{\mathbf{x}}| - \frac{1}{4}\right) \\ &= \frac{1}{2}a^2 \ln a - \frac{1}{2}|\bar{\mathbf{x}}|^2 \ln|\bar{\mathbf{x}}| + \frac{1}{4}|\bar{\mathbf{x}}|^2 - \frac{1}{4}a^2. \end{aligned} \tag{136}$$

So,

$$\begin{aligned} &\frac{1}{2}\int_{\Omega_e^c} \ln(1+t^2-2t\cos\phi)\, d\Omega \\ &= \frac{\pi}{2}(2a^2 \ln a - 2a^2 \ln|\bar{\mathbf{x}}| + |\bar{\mathbf{x}}|^2 - a^2). \end{aligned} \tag{137}$$

So,

$$\begin{aligned} &\int_{\Omega_e^c} \ln|\mathbf{r}| \delta_{im}\, d\Omega \\ &= \int_{\Omega_e^c} \ln|\bar{\mathbf{x}}| \delta_{im}\, d\Omega + \frac{1}{2}\int_{\Omega_e^c} \ln(1+t^2-2t\cos\phi)\delta_{im}\, d\Omega \\ &= \left[\frac{\pi}{2}(2a^2 \ln a - 2a^2 \ln|\bar{\mathbf{x}}| + |\bar{\mathbf{x}}|^2 - a^2) + \pi a^2 \ln|\bar{\mathbf{x}}|\right]\delta_{im} \\ &= \left[\frac{\pi}{2}(|\bar{\mathbf{x}}|^2 - a^2) + \pi a^2 \ln a\right]\delta_{im}. \end{aligned} \tag{138}$$

So we can have the final result

$$\begin{aligned} &\int_{\Omega_e^c} v^*_{mi}(\bar{\mathbf{x}} - \bar{\mathbf{y}})\, d\Omega_{\bar{\mathbf{y}}} \\ &= \frac{1}{4\pi\nu}\int_{\Omega_e^c}\left(\frac{(\bar{x}_i - \bar{y}_i)(\bar{x}_m - \bar{y}_m)}{|\bar{\mathbf{x}} - \bar{\mathbf{y}}|^2} - \ln|\bar{\mathbf{x}} - \bar{\mathbf{y}}|\delta_{im}\right) d\Omega \\ &= \frac{1}{8\nu}\bar{x}_i\bar{x}_m + \frac{1}{8\nu}a^2\delta_{im} - \frac{1}{16\nu}|\bar{\mathbf{x}}|^2\delta_{im} \\ &\quad - \left[\frac{1}{8\nu}(|\bar{\mathbf{x}}|^2 - a^2) + \frac{1}{4\nu}a^2 \ln a\right]\delta_{im} \\ &= \frac{1}{8\nu}\bar{x}_i\bar{x}_m + \frac{\delta_{im}}{4\nu}\left[a^2(1 - \ln a) - \frac{3}{4}|\bar{\mathbf{x}}|^2\right]. \end{aligned} \tag{139}$$

Now we move to the **F** tensor. We first need the derivative of the Green's function (114). Simple calculation gives us

$$v^*_{im,j}(\bar{\mathbf{x}} - \bar{\mathbf{y}}) = \frac{1}{4\pi\nu}\left[\frac{1}{|\mathbf{r}|^2}(r_i\delta_{mj} + r_m\delta_{ij} - r_j\delta_{im}) - \frac{2}{|\mathbf{r}|^4}r_i r_m r_j\right], \tag{140}$$

where $\mathbf{r} = \bar{\mathbf{x}} - \bar{\mathbf{y}}$. Define $\ell_i = -r_i/|\mathbf{r}|$ as before, we have

$$v^*_{im,j} = \frac{1}{4\pi\nu|\mathbf{r}|}(2\ell_i\ell_m\ell_j - (\ell_i\delta_{mj} + \ell_m\delta_{ij} - \ell_j\delta_{im})). \tag{141}$$

With similar procedures as earlier, the integral of $v^*_{im,j}$ over the local domain can be carried out as

$$\int_{\Omega_e^c} v^*_{im,j}\,\mathrm{d}\Omega = \frac{1}{4\pi\nu}\int_0^{2\pi}\int_0^{R(\ell)}\left[\frac{2}{|\mathbf{r}|}\ell_i\ell_m\ell_j - \frac{1}{|\mathbf{r}|}(\ell_i\delta_{mj}+\ell_m\delta_{ij}-\ell_j\delta_{im})\right]|\mathbf{r}|\,\mathrm{d}|\mathbf{r}|\,\mathrm{d}\theta = \frac{1}{4\pi\nu}\int_0^{2\pi}(-\ell_k\bar{x}_k) \times (2\ell_i\ell_m\ell_j-\ell_m\delta_{ij}-\ell_j\delta_{im})\,\mathrm{d}\theta. \quad (142)$$

Exploiting the identities (124) and (125), (142) becomes

$$\int_{\Omega_e^c} v^*_{im,j}\,\mathrm{d}\Omega_y = \frac{1}{8\nu}(\delta_{ij}\bar{x}_m+\delta_{jm}\bar{x}_i-3\delta_{im}\bar{x}_j). \quad (143)$$

Now we can get the explicit form of the **F** tensor based on (143)

$$F_{ijm} = \int_{\Omega_e^c}\frac{1}{2}(v^*_{im,j}+v^*_{jm,i})\,\mathrm{d}\Omega_y = \frac{1}{8\mu}[\delta_{ij}\bar{x}_m-(\delta_{jm}\bar{x}_i+\delta_{im}\bar{x}_j)]. \quad (144)$$

We now evaluate the vector **e**, the 2-D pressure Green's function is given as follows:

$$p^*_i(\bar{\mathbf{x}}-\bar{\mathbf{y}}) = \frac{r_i}{2\pi|\mathbf{r}|^2}. \quad (145)$$

Then we have

$$e_i = \int_{\Omega_e^c} p^*_i\,\mathrm{d}\Omega_{\bar{y}} = \int_{\Omega_e^c}\frac{r_i}{2\pi|\mathbf{r}|^2}\,\mathrm{d}\Omega = \frac{1}{2\pi}\int_0^{2\pi}\int_0^{R(\ell)}\frac{\ell_i}{|\mathbf{r}|}|\mathbf{r}|\,\mathrm{d}|\mathbf{r}|\,\mathrm{d}\theta = \frac{1}{2\pi}\int_0^{2\pi}-(\ell_k\bar{x}_k)\ell_i\,\mathrm{d}\theta = -\frac{\bar{x}_i}{2}. \quad (146)$$

This ends the derivations for **T**, **F** and **e**.

References

[1] A.N. Brooks, T.J.R. Hughes, Streamline upwind/Petrov–Galerkin formulations for convection dominated flows with particular emphasis on the incompressible Navier–Stokes equations, Comput. Methods Appl. Mech. Eng. 32 (1982) 199–259.

[2] T.J.R. Hughes, L. Franca, G. Hulbert, A new finite element formulation for fluid dynamics: VIII. The Galerkin least-squares method for advective–diffusive equations, Comput. Methods Appl. Mech. Eng. 73 (1989) 173–189.

[3] T.J.R. Hughes, Multiscale phenomena: Green's functions, the Dirichlet-to-Neumann formulation, subgrid scale models, bubbles and the origins of stabilized methods, Comput. Methods Appl. Mech. Eng. 127 (1995) 387–401.

[4] T.J.R. Hughes, G. Feijoo, L. Mazzei, J.-B. Quincy, The variational multiscale method: a paradigm for computational mechanics, Comput. Methods Appl. Mech. Eng. 166 (1998) 3–24.

[5] G. Hauke, A. Garcia-Olivares, Variational subgrid scale formulations for the advection–diffusion-reaction equation, Comput. Methods Appl. Mech. Eng. 190 (2001) 6847–6865.

[6] T.J.R. Hughes, L. Mazzei, K.E. Jansen, Large eddy simulation and the variational multiscale method, Comput. Vis. Sci. 3 (2000) 47.

[7] K. Garikipati, T.J.R. Hughes, A variational multiscale approach to strain localization-formulation for multidimensional problems, Comput. Methods Appl. Mech. Eng. 188 (2000) 39–60.

[8] R. Juanes, A Variational Multiscale Method for the Numerical Simulation of Multiphase Flow in Porous Media, Computational Methods in Water Resources XV, vol. 1, Elsevier, Amsterdam, 2004, pp. 325–335.

[9] S. Li, A. Gupta, X. Liu, M. Mahyari, Variational eigenstrain multiscale finite element method, Comput. Methods Appl. Mech. Eng. 193 (2004) 1803–1824.

[10] S. Li, X. Liu, A. Gupta, Smart element method I. The Zienkiewicz–Zhu feedback, Int. J. Numerical Methods Eng. 62 (2005) 1264–1294.

[11] O. Pironnear, Finite Element Methods for Fluids, Wiley, New York, 1989.

[12] S.C. Brenner, L.R. Scott, The Mathematical Theory of Finite Element Methods, second ed., Springer, New York, 2002.

[13] T.J.R. Hughes, The Finite Element Method, Prentice-Hall, Englewood Cliffs, NJ, 1987.

[14] F. Brezzi, M. Fortin, Mixed and Hybrid Finite Element Methods, Springer, Berlin, 1991.

[15] S. Norburn, D. Silvester, Stabilised vs. stable mixed methods for incompressible flow, Comput. Methods Appl. Mech. Eng. 166 (1998) 131–141.

[16] D.N. Arnold, F. Brezzi, M. Fortin, A stable finite element for the Stokes equations, Calcolo 23 (1984) 337–344.

[17] E. Onãte, J. Garcia, S. Idelsohn, Computation of the stabilization parameter for the finite element solution of advective–diffusive problems, Int. J. Numerical Methods Fluids 25 (1997) 1385–1407.

[18] J. Donea, A. Huerta, Finite Element Methods for Flow Problems, Wiley, New York, 2003.

[19] L. Franca, T.J.R. Hughes, Convergence analyses of Galerkin least-squares methods for symmetric advective–diffusive forms of the Stokes and incompressible Navier–Stokes equations, Comput. Methods Appl. Mech. Eng. 105 (1993) 285–298.

[20] O.A. Ladyzhenskaya, The Mathematical Theory of Viscous Incompressible Flow, second English ed., Gordon and Breach Science, New York, 1969.

[21] L.C. Wrobel, The Boundary Element Method, Applications in Thermo-Fluids ad Acoustics, vol. 1, Wiley, New York, 2001.

[22] D. Krajcinovi, Damage Mechanics, Elsevier, New York, 1996.

[23] L.S. Gradsbteyn, L.M. Ryzbik, Table of Integrals, Series and Products, sixth ed., Academic Press, New York, 2000.